


A SPECTRAL-SPATIAL FUSION ANOMALY DETECTION METHOD FOR HYPERSPECTRAL IMAGERY

A PREPRINT

 **Zengfu Hou***
School of Information and Electronics
Beijing Institute of Technology
Beijing, 100081
zephyrhoul26.com

Siyuan Cheng
Space star technology co., LTD
Beijing, 100086
347707597@qq.com

Ting Hu†
School of Information and Electronics
Beijing Institute of Technology
Beijing, 100081
ht_hc2@163.com

February 25, 2022

ABSTRACT

In hyperspectral, high-quality spectral signals convey subtle spectral differences to distinguish similar materials, thereby providing unique advantage for anomaly detection. Hence fine spectra of anomalous pixels can be effectively screened out from heterogeneous background pixels. Since the same materials have similar characteristics in spatial and spectral dimension, detection performance can be significantly enhanced by jointing spatial and spectral information. In this paper, a spectral-spatial fusion anomaly detection (SSFAD) method is proposed for hyperspectral imagery. First, original spectral signals are mapped to a local linear background space composed of median and mean with high confidence, where saliency weight and feature enhancement strategies are implemented to obtain an initial detection map in spectral domain. Furthermore, to make full use of similarity information of local background around testing pixel, a new detector is designed to extract the local similarity spatial features of patch images in spatial domain. Finally, anomalies are detected by adaptively combining the spectral and spatial detection maps. The experimental results demonstrate that our proposed method has superior detection performance than traditional methods.

Keywords Hyperspectral · Anomaly detection · Saliency weight · Feature enhancement · Adaptive fusion

1 Introduction

Hyperspectral images (HSI) are different from multispectral or panchromatic images, which record not only spatial distribution information of objects but also its spectral structure information. Hence, different materials can be distinguished by using their spectral features Hou et al. [2018], Hou and Li [2022]. These distinctive fine spectra like human fingerprints with uniqueness have shown great potential in target detection applications Zhao et al. [2021].

However, prior knowledge of target spectrum is difficult to obtain in advance, which limits its application scenarios. In practical terms, by only analyzing spectral signals of hyperspectral images, it is possible to identify different objects. Therefore, hyperspectral imaging has shown great potential applications for various scenarios, such as scene classification Hu et al. [2017], spectral unmixing Villa et al. [2010], change detection Hou et al. [2021a,b], target detection Zhao et al. [2021], and anomaly detection Liu et al. [2021], Hou et al. [2020], etc.. Among these applications, anomaly detection has gotten a lot of attention due to its ability to recognize objects differing from the surrounding background only using spectral differences rather than prior spectrum Hou et al. [2021c].

Hyperspectral anomaly detection aims to identify objects of interest that are spatially or spectrally different from its surrounding. Therefore, how to effectively select and mark anomalous pixels from an entire image has become the main challenge. For this challenge, various statistical and physical models have been reported.

*website: <https://zephyrhours.github.io>

†Corresponding author

Assuming that background obeys multivariate Gaussian normal distribution, well-known Reed-Yu (RX) Reed and Yu [1990] algorithm is proposed, where Mahalanobis distance is calculated to measure the similarity between testing pixel and background ones. When the whole image is considered as Gaussian background model, it is called global RX (GRX) Reed and Yu [1990]. If RX detector estimates background model using local statistics, it is called local RX (LRX) Molero et al. [2013]. However, the background cannot be simply described with a multivariate normal distribution because of its extremely complicated distribution. Therefore, some improved RX-based methods such as weighted RX (WRX) Guo et al. [2014], linear filter RX (LFRX) Guo et al. [2014], and kernel RX (KRX) Kwon and Nasrabadi [2005] are investigated.

Compared with the above background statistics-based methods, some linear representation-based methods producing better detection performance have been proposed. For example, the collaborative representation detector (CRD) Li and Du [2014] exploiting the similarity relationship between non-anomalous pixel and background pixels had achieved satisfactory detection performance, which represented the testing pixel linearly via its neighborhood pixels. However, the outliers in background pixels could degrade the representation accuracy. To generate relatively pure background pixels, a CRD with outlier removal anomaly detector (CRDBORAD) Vafadar and Ghassemian [2017] was proposed, removing some suspected anomaly pixels. Subsequently, a CRD combined with principal component analysis (PCARCRD) Su et al. [2018] was put forward, where principal component analysis (PCA) was used for outlier removal. Considering the contributions of spatial information, a CRD-based local summation and inverse distance weight detector (LSADCRIDW) Tan et al. [2019a] was proposed to makes full use of the various local spatial distribution information of the neighboring pixels. Utilizing the least squares technique to purify background pixels as well as weighting the average saliency of the neighboring pixels into the detection map, CRD with background purification and saliency weight [10] (CRDBPSW) was put forward.

The third anomaly detection method, as the low-rank matrix decomposition serves as a powerful tool to exploit the intrinsic low-rank property of images Candès et al. [2011]. These low rank representation (LRR)-based methods aim to find a low-dimensional subspace to represent the entire image with as few as possible atoms. Assume that the background pixel obeyed a single subspace, the classical robust principal component analysis (RPCA) Candès et al. [2011] method that decomposed the image matrix into a low-rank matrix and a sparse matrix, was proposed, where the sparse matrix was used for anomaly detection Liu et al. [2012]. By applying the RX detector to the sparse matrix, the RPCA-RX Liu et al. [2012] detector was proposed to perform anomaly detection. Different from RPCA, the LRR model used multiple subspaces to represent the data, with being more suitable for an HSI with complex background features. Subsequently, by adding a sum-to-one constraint, the low-rank representation sum-to-one (LRRSTO) Xu et al. [2015a] mode was proposed for anomaly detection. Considering that the direct application of LRR model was sensitive to a tradeoff parameter, the LRR-based and Learned Dictionary (LRRaLD) Niu and Wang [2016] method was proposed, where the dictionary was learned from the entire image with a random selection processing. To make full use of the local background statistics information, single/multiple local windows-based LRRSTO (SLW/MLW_LRRSTO) Tan et al. [2019b] method was proposed. As yet, many LRR-based methods, such as sparse representation (SRD) Chen et al. [2011], low-rank and sparse representation (LRASR) Xu et al. [2015b], and graph total variation regularized low rank representation (GTVLRR) Cheng and Wang [2019], etc. have been published with better detection results.

Recently, deep learning-based methods have drawn increasing attention in hyperspectral anomaly detection. A transferred deep convolutional neural network detector (CNND) Li et al. [2017] was the first attempt to train an anomaly detector using pixel pairs selected from a reference data. With the birth of autoencoders (AEs), various AEs such as spectral constrained adversarial AE (SC_AAE) Xie et al. [2019], stacked denoising AEs (SDAs) Zhao and Zhang [2018], and manifold-constrained AE network Lu et al. [2019], etc. were introduced into hyperspectral anomaly detection Wang et al. [2022], Zhao et al. [2017]. They usually achieved outstanding judge for anomalous pixels via the spectral signal; nevertheless, the spatial features were ignored.

To address the above problems, an effective spectral-spatial fusion anomaly detection (SSFAD) framework is designed in this paper. In the spectral domain, a local median-mean line (LMML) projection method is proposed, where local adjacent pixels surrounding the testing pixel are mapped into the median-mean line to rectify the position of the background samples. In addition, a monotonic increasing function based on inverse distance weight (IDW) Tan et al. [2019a] is used to further increase the gap between the anomalous and the local background pixels. The spectral feature map is obtained by a saliency weight-based detector. In the spatial domain, a local spatial similarity measurement method is proposed to fully use of spatial similarity features of local background. Finally, an adaptive score strategy is proposed to determine the fusion coefficients of the two complementary parts.

The main contributions can be summarized as follows.

- 1) A novel dual-pipeline framework is proposed for hyperspectral anomaly detection, where spectral and spatial features are fused by the proposed adaptive score strategy to further highlight anomaly.

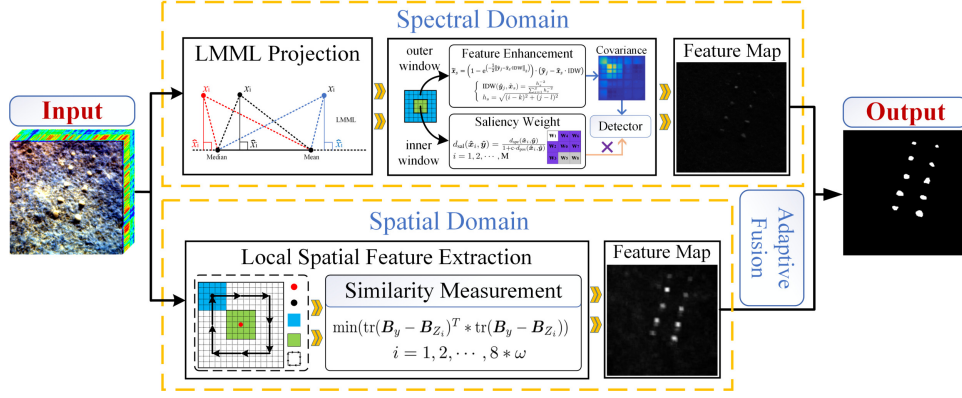
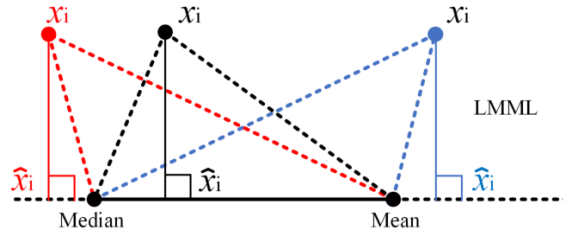


Figure 1: Framework of proposed SSFAD detector for hyperspectral anomaly detection.

Figure 2: Illustration of the projection of testing pixel x_i on LMML.

2) In spectral domain, LMML projection and feature enhancement strategies were proposed to increase the discrimination between anomalous and background pixels.

3) When extracting spatial features, a local spatial similarity measurement method is designed to improve the detection effect by exploiting intrinsic local pixels relation.

The remainder of this article is organized as follows. In Section II, a detailed description of the proposed framework is presented. In Section III, four real datasets are utilized to verify the proposed method, and the parameters and results are analyzed and discussed. The conclusion is drawn in Section IV.

2 Proposed Detection Method

During background modeling in traditional methods, anomalous pixels are judged by the spectral signals, while the spatial features were ignored. Homogeneous pixels in the background may affect the detection performance. Thus, it is necessary to maximize the spatial texture between background and anomaly. Fig. 1 displays a flowchart of the proposed SSFAD framework, which consists of the following steps. To begin, spectral feature map is obtained by LMML, feature enhancement and saliency weight strategies. After that, spatial feature map is extracted by local spatial similarity measurement. Finally, two complementary detection maps are adaptive fused to highlight anomaly.

2.1 Spectral Domain-Based Anomaly Feature Extraction

In anomaly detection, covariance statistic-based methods rely excessively on the accuracy of background statistics. In hyperspectral imaging, the spectral curve is easily disturbed by various complex factors such as noise and dark current causing the oscillation of spectral curves. Moreover, in real scenarios, anomalous targets play outlier roles to contaminate the background data, which hinders the accurate estimation of the background pixels. Both phenomena could seriously degrade the performance of covariance statistic-based anomaly detection methods. In this paper, to degrade the negative effect on the mean and covariance matrix caused by anomalous pixels Imani [2017], a LMML projection method is proposed to rectify the position of background samples. Specifically, all the neighborhood pixels inside the outer window ω_{out} of testing pixel are projected into LMML space.

$$\hat{x}_i = (1 - \eta_i)\mathbf{M} + \eta_i\mathbf{m}, i = 1, 2, \dots, N, \quad (1)$$

where M and m are the median value and mean value, respectively. $\eta_i \in [0, 1]$ denotes the position parameter. $N = \omega_{\text{out}} * \omega_{\text{out}}$, which represents the number of pixels in the local window centered on the testing pixel x_i . As shown in Fig. 2, the connecting line between pixel x_i and its projection point \hat{x}_i is perpendicular to the median-mean line. According to the geometric theory, there is,

$$[(1 - \eta_i)M + \eta_i m - x_i] \cdot (m - M) = 0, \quad (2)$$

then,

$$\eta_i = \frac{(x_i - M) \cdot (m - M)}{(m - M) \cdot (m - M)}, \quad i = 1, 2, \dots, N. \quad (3)$$

After the LMML operation, local pixels are mapped in the median-mean direction, while outliers are distributed in sides of the median-mean line. The farther away from the median and mean points, the higher the probability of anomalies. Furthermore, an adaptive local background prototype is obtained via the LMML projection, where the projection point of each pixel is used as the rectified background pixels to calculate the local covariance matrix.

Inspired by Lei et al. [2019], where a suppression function is used to construct a discriminative feature space. Hence, to further enlarge the difference between background and anomalous pixels, a novel monotonic increasing function is proposed, which is formulated as,

$$\begin{cases} \tilde{x}_s = (1 - \exp(-\frac{1}{2} \|\hat{y}_j - \hat{x}_s \cdot \text{IDW}\|_2)) \cdot (\hat{y}_j - \hat{x}_s \cdot \text{IDW}) \\ s = 1, 2, \dots, S \end{cases}, \quad (4)$$

where \hat{y}_j and \hat{x}_s represent the projection vectors of the testing pixel and its neighborhood pixels between the outer window ω_{out} and the inner window ω_{in} in LMML space, respectively. $S = \omega_{\text{out}} * \omega_{\text{out}} - \omega_{\text{in}} * \omega_{\text{in}}$, which is the number of neighborhood pixels. IDW denotes the inverse distance weight Tan et al. [2019a], which is used to make the most of the space-varying information where the closer the testing pixel is, the higher the similarity between the background pixels and the testing pixel will be. It is formulated as,

$$\begin{cases} \text{IDW}(\hat{y}_j, \hat{x}_s) = \frac{h_s^{-2}}{\sum_{s=1}^S h_s^{-2}} \\ h_s = \sqrt{(i-k)^2 + (j-l)^2} \end{cases}, \quad (5)$$

where (i, j) and (k, l) denote the geometric coordinates of testing pixel \hat{y}_j and its any neighborhood pixel \hat{x}_s , respectively. The feature map in spectral domain is obtained by,

$$r = \hat{y} \Sigma^{-1} \hat{y}^T \quad (6)$$

where Σ denotes the covariance matrix of the local background pixels \tilde{x}_s between the inner window and the outer window.

In addition, considering the influence of adjacent pixels contained in an inner window on the testing pixel, a saliency weight Hou et al. [2021c] is used,

$$\begin{cases} d_{\text{sal}}(\hat{x}_i, \hat{y}) = \frac{d_{\text{spe}}(\hat{x}_i, \hat{y})}{1 + c \cdot d_{\text{pos}}(\hat{x}_i, \hat{y})} \\ i = 1, 2, \dots, M \end{cases}, \quad (7)$$

where d_{sal} denotes the saliency distance between the testing pixel \hat{y} and its any neighborhood pixel \hat{x}_i contained in the inner window. $M = \omega_{\text{in}} * \omega_{\text{in}} - 1$ is the number of adjacent pixels contained in the inner window. c is a constant that could cause little effect on the result. As suggested by Hou et al. [2021c], its value is set to 1. d_{spe} and d_{pos} represent the spectral distance and position distance respectively, which are formulated as,

$$d_{\text{spe}}(\hat{x}_i, \hat{y}) = \arccos\left(\frac{\hat{x}_i \hat{y}}{\|\hat{x}_i\|_2 \cdot \|\hat{y}\|_2}\right), \quad (8)$$

$$d_{\text{pos}}(\hat{x}_i, \hat{y}) = \sqrt{(i-k)^2 + (j-l)^2}. \quad (9)$$

Finally, average all saliency distances to produce the saliency weight of the testing pixel,

$$w_{\text{sal}} = \frac{\sum_{i=1}^M d_{\text{sal}}}{M}. \quad (10)$$

When the spectral signal of testing pixel is significantly different from that of its adjacent pixels, the pixel is regional saliency. Therefore, the final detection result in spectral domain is reformulated as,

$$r_1 = \hat{y} \Sigma^{-1} \hat{y}^T \cdot w_{\text{sal}}. \quad (11)$$

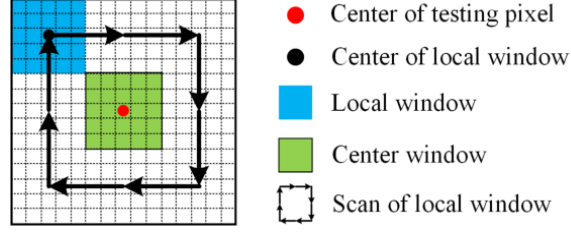


Figure 3: Illustration of calculating pixel's local spatial features.

2.2 Spatial Domain-Based Anomaly Feature Extraction

If the testing pixel is anomalous, its spatial structure would differ from ones of the neighborhood background Ju et al. [2018]. To calculate the spatial structure similarity between the testing pixel and its neighborhood background, a novel local spatial similarity measurement method is formulated as,

$$\begin{cases} r_2 = \min(\text{tr}(\mathbf{B}_y - \mathbf{B}_{Z_i})^T * \text{tr}(\mathbf{B}_y - \mathbf{B}_{Z_i})) \\ i = 1, 2, \dots, 8 * \omega \end{cases}, \quad (12)$$

where \mathbf{B}_y denotes the center window (see the green window in Fig. 3) centered on testing pixel, \mathbf{B}_{Z_i} is the neighborhood background window (highlighted as the blue window in Fig. 3), and ω represents the size of spatial structure window.

The local spatial similarity of the center window is calculated following Fig. 3. By sliding the blue window clockwise around the green window, the local spatial similarity information around the center window is obtained. Theoretically, different sizes and shapes should be selected for the spatial structure window for a better adaption to the local characteristics in images. For simplicity, the inner green window is regarded as the spatial structure window. In addition, the size of local background window is set as ω . The most similar spatial structure window are searched from its background area. By Eq. 12, the spatial structure similarity between center window around testing pixel and its neighborhood background windows is obtained. The bigger the similarity, the smaller the value, and the more likely it is to be background, and vice versa.

2.3 Spectral-Spatial Fusion Anomaly Detection

To highlight anomalous targets, two complementary detection maps are adaptively fused. Single feature cannot detect anomaly well in complex scenario, therefore, a fusion strategy is adopted here. A linear score function shown in Eq.13 is employed as the fusion strategy.

$$R = a * R_1 + b * R_2, \quad (13)$$

where R is the finally anomaly detection result. a and b are the corresponding weight factors. It is difficult to tune a and b experientially to obtain an optimal value, and a general option is the average pooling operation. That is, $a = b = 0.5$. In this paper, a score mechanism is proposed to adaptively determine the values of a and b , which is formulated as,

$$\begin{cases} a = \frac{\sqrt{\lambda_{\max}(R_1^T R_1)}}{\sqrt{\lambda_{\max}(R_1^T R_1) + \sqrt{\lambda_{\max}(R_2^T R_2)}}} \\ b = \frac{\sqrt{\lambda_{\max}(R_2^T R_2)}}{\sqrt{\lambda_{\max}(R_1^T R_1) + \sqrt{\lambda_{\max}(R_2^T R_2)}}} \end{cases}, \quad (14)$$

where $\lambda_{\max}(\cdot)$ takes the maximal eigenvalue of an matrix. Such adaptive score strategy could help to increase the detection performance.

3 Experiments and Discussion

3.1 Datasets Description

In this section, to evaluate the performance of the proposed detector, experiments are conducted on four hyperspectral images. The first image Kang et al. [2017] was obtained by airborne visible/infrared imaging spectrometer (AVIRIS) sensor over Gulfport area on July 7, 2010. This Gulfport image with spatial resolution of 3.4 m, consists of 100×100 pixels and 191 spectral bands after removing the invalid bands, where the anomalies refer to the airplanes. The scenario and its ground-truth map are shown in Fig. 4(a) and Fig.4(e).

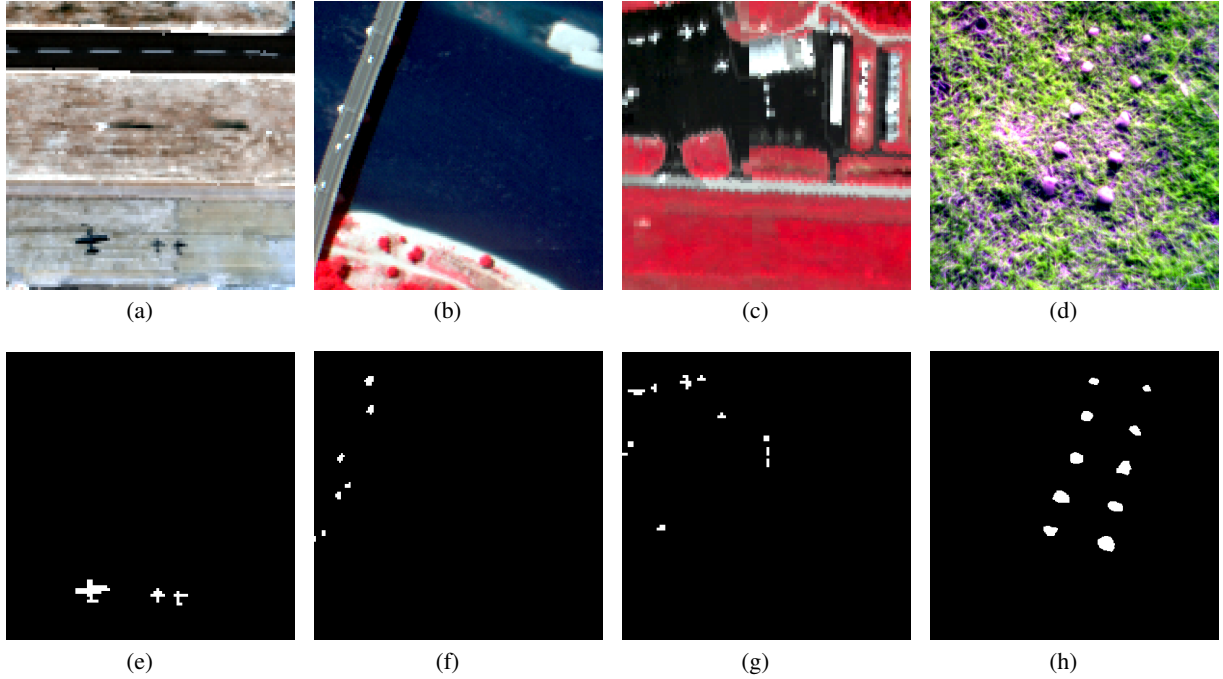


Figure 4: The pseudo color presentation of (a) Gulfport, (b) Pavia Centra, (c) Gainesville, (d) Cri; the ground-truth map of (e) Gulfport, (f) Pavia Centra, (g) Gainesville, (h) Cri.

Table 1: The optimal parameters of various detectors in different datasets.

Methods	Gulfport	Pavia Centra	Gainesville	Cri
LRX	(17,15)	(25,5)	(9,7)	(19,15)
CRD	(23,15,10 ⁻⁶)	(7,5,10 ⁻⁶)	(9,7,10 ⁻⁶)	(19,9,10 ⁻⁶)
RPCA-RX	0.01	0.01	0.01	0.001
GTVLRR	(0.5,0.2,0.1)	(0.7,0.4,0.05)	(0.005,1,0.5)	(0.005,1,0.5)
2S-GLRT	(13,11)	(21,5)	(9,5)	(25,15)
SSFAD	(5,3)	(5,3)	(5,3)	(17,15)

The second image Kang et al. [2017], Bitar et al. [2019] was acquired by the Reflective Optics System Imaging Spectrometer (ROSIS) airborne sensor during a flight campaign over Pavia, northern Italy. Its size and geometric resolution are $150 \times 150 \times 115$ and 1.3 m, respectively. 102 bands are retained as the noisy bands are discarded. The Pavia Centra image mainly contains a background of water and a bridge and some anomalies of vehicles, of which the scenario and the ground-truth map are given in Fig. 4(b) and Fig. 4(f).

The third dataset Kang et al. [2017] of spatial resolution 3.5 m is an urban scene of Gainesville located on the north central of Florida, USA, obtained by AVIRIS on September 4, 2010. It consists of 191 image bands of size 100×100 . Fig. 4(c) and Fig. 4(g) depict the Gainesville image and its corresponding ground truth, respectively.

The fourth dataset Huyan et al. [2018], Zhang et al. [2015] was acquired by the Nuance Cri Hyperspectral sensor at the spectral resolution of 10 m and in the wavelength range of [650, 1100] nm. The Cri image of size $400 \times 400 \times 46$ captures a grassland corrupted by 10 rock anomalies of pixel 2261. The pseudo color image is shown in Fig. 4(d), while the contained anomalies can be clearly observed in Fig. 4(h).

Table 2: AUC values (%) of different fusion strategies in SSFAD. The maximum value is highlighted by red

Methods	Gulfport	Pavia Centra	Gainesville	Cri
average pooling	99.309	99.843	98.903	99.614
adaptive score	99.307	99.882	98.970	99.751

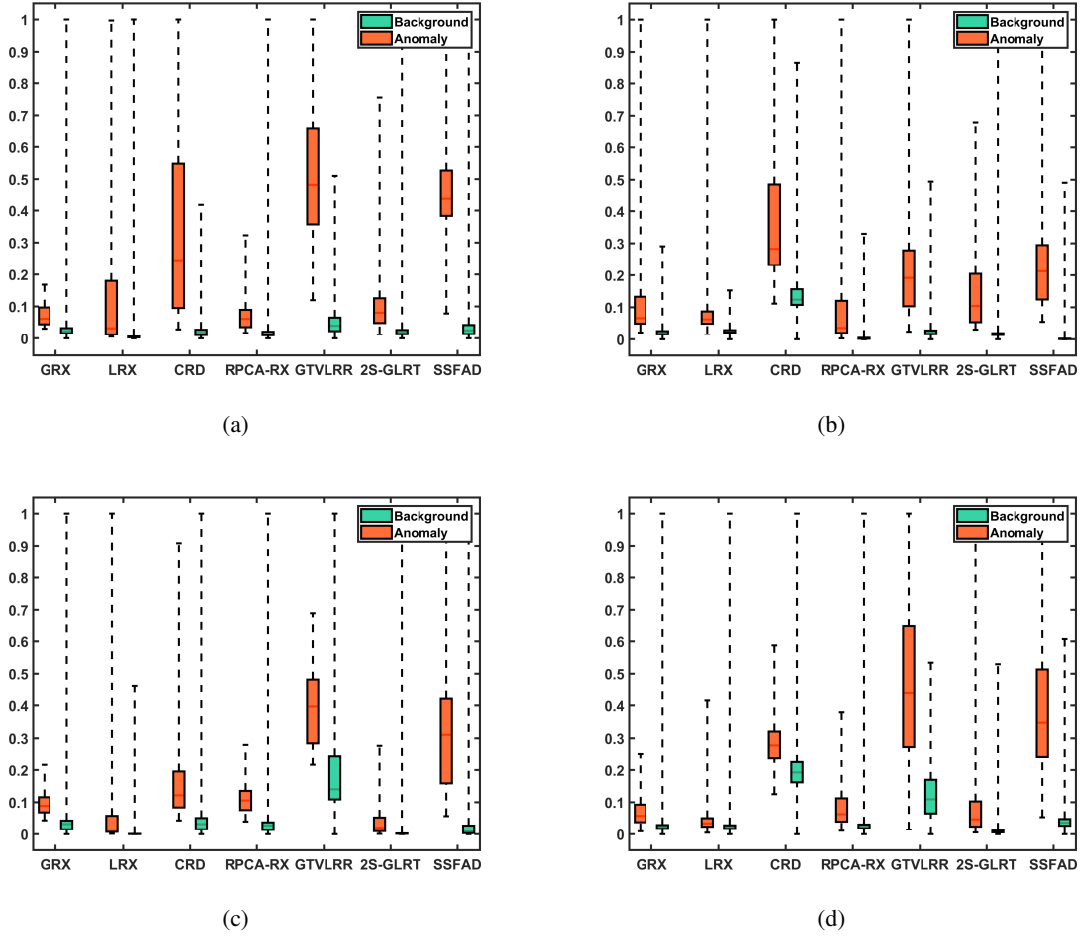


Figure 5: Statistical separability analysis for different datasets: (a) Gulfport; (b) Pavia Centra; (c) Gainesville; (d) Cri.

3.2 Parameters setting

To effectively verify the performance of the proposed SSFAD method, six widely-used anomaly detectors, e.g. GRX, LRX, CRD, RPCA-RX, GTVLRR and 2S-GLRT, are employed for evaluation. Meanwhile, for qualitative and quantitative comparisons, statistical separability analysis Hou et al. [2021c], receiver operating characteristic (ROC) Hanley and McNeil [1982] and area under the curve (AUC) metric are utilized as the main criteria.

The choices of parameters are important for these methods with parameters, by which its detection performance is greatly affected. For a fair comparison, the parameters of all considered methods are carefully tuned following their experiences, to generate their best detection results. As suggested in Liu et al. [2021], Hou et al. [2021c], for the LRX and SSFAD, by varying the outer window size ω_{out} from 5 to 25 and the inner window size ω_{in} from 3 to 15, the optimal detection performance under different window sizes ($\omega_{out}, \omega_{in}$) is collected. For the CRD, by fixing λ as 10^{-6} and varying ω_{out} from 5 to 25 and ω_{in} from 3 to 15, the optimal detection performance under different window sizes is selected. For the RPCA-RX, the optimal parameter λ is selected from 10^{-4} to 10^4 for comparative experiments. As to the GTVLRR, the K-means method is used to construct dictionary referring to Cheng and Wang [2019], Liu et al. [2021], and empirical parameters (λ, β, γ) are firstly set to (0.5, 0.2, 0.05). Then, by fixing β and γ , and varying λ in [0.005, 0.05, 0.1, 0.3, 0.5, 0.7, 1], the optimal λ under different values is selected. Similarly, by fixing the selected λ and default γ , and varying β in [0.005, 0.05, 0.1, 0.2, 0.4, 0.7, 1], the optimal β is selected. In the same way, the optimal γ is selected in [0.005, 0.01, 0.02, 0.05, 0.1, 0.2, 0.5]. The optimal parameters of various detectors are listed in Table 1.

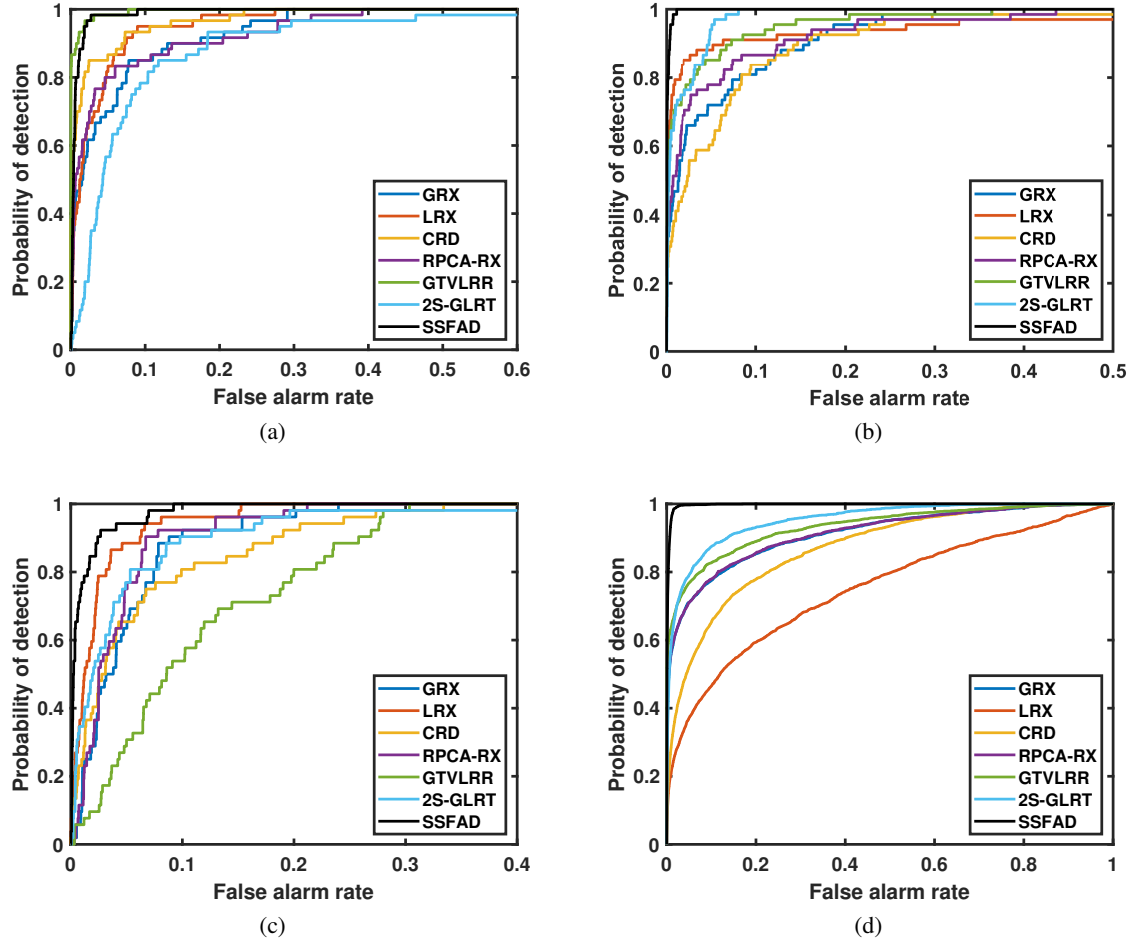


Figure 6: ROC curves for different datasets: (a) Gulfport; (b) Pavia Centra; (c) Gainesville; (d) Cri.

Table 3: AUC values (%) of various anomaly detectors using different datasets. The top two values are highlighted by red and blue

Methods	Gulfport	Pavia Centra	Gainesville	Cri
GRX	95.260	95.380	95.128	91.342
LRX	96.942	95.973	97.690	75.251
CRD	97.927	94.072	93.930	87.267
RPCA-RX	95.348	95.906	95.861	91.478
GTVLRR	99.691	97.636	88.604	93.429
2S-GLRT	91.831	98.676	94.856	95.403
SSFAD	99.307	99.882	98.970	99.751

Table 4: Execution time of various anomaly detectors using different datasets (unit: seconds).

Methods	Gulfport	Pavia Centra	Gainesville	Cri
GRX	0.08	0.08	0.12	0.32
LRX	39.57	50.98	34.14	91.59
CRD	69.97	4.79	3.87	866.59
RPCA-RX	2.61	2.19	2.56	7.76
GTVLRR	61.06	88.89	49.40	981.47
2S-GLRT	74.36	48.11	36.60	4272.53
SSFAD	50.44	44.67	47.67	3197.97

3.3 Detection Performance

Statistical separability analysis Liu et al. [2021], Zhao et al. [2021], also known as boxplot, has been widely used as a performance assessment in hyperspectral anomaly detection, target detection, and change detection. Essentially, the boxplot is used to reflect the distribution characteristics of various detection results, where the separation degree between different categories is judged by the interval between different boxes. Herein, the separability and the suppression level between anomaly and background is evaluated by statistical separability analysis, where the red and green boxes represent the anomalous and background pixels, respectively. The interval between the red and green box represents the separability between the anomalous and background pixels, while the height of the green box means the suppression degree of these methods to the background. Generally, a shorter green box corresponds to a stronger background suppression, reflecting a better separation for background and anomaly.

The detection performance of the considered algorithms on four experimental datasets is displayed. As can be seen from Fig. 5(a) that the intervals between the red and green boxes of SSFAD and GTVLRR are larger than those of the GRX, LRX, CRD, RPCA-RX and 2S-GLRT, which indicates that both methods can separate the anomalies well from the background. In addition, SSFAD is slightly better than GTVLRR towards interval, and perform the shortest green box. Thus, this proposed method can suppress the background better in the Gulfport dataset. Fig. 5(b) shows that except CRD, the compared detectors can effectively suppress the background of the Pavia Centra dataset. Obviously, SSFAD achieves the best separability than the others. From Fig. 5(c) and Fig. 5(d), it can be seen that SSFAD produces the widest interval when compared with other six detectors, i.e., GRX, LRX, CRD, RPCA-RX, GTVLRR and 2S-GLRT. Comprehensively, the proposed SSFAD can separate anomalies from background more effectively.

For an accuracy evaluation, the ROC curves of each detector on the experimental images are plotted in Fig. 6. The closer the curve is to the upper left corner, the better the detection performance. As Fig. 6(a) depicted, the GRX shows the worst performance. The green and black curves are closer to the upper left corner than others, representing that GTVLRR and the proposed SSFAD both achieve good detection performance, and GTVLRR is slightly better than SSFAD. The experimental results shown in Figs. 6(b)-(d) reveal the obvious advantage of the proposed SSFAD when detecting the Pavia Centra, Gainesville, and Cri dataset, because the black curve is closest to the upper left corner.

The AUC values of different fusion strategies are compared in Table 2. Obviously, the proposed adaptive score strategy achieves better results than the average pooling strategy, especially in Cri dataset. This also further confirms that the adaptive score strategy can better highlight anomaly than the average pooling strategy. In addition, the AUC values of various methods on different datasets are listed in Table 3. By comparing these AUC values, the almost best performance of proposed SSFAD can be observed. Especially on the Cri dataset, the improvement of SSFAD approximates to 4% when compared with the second best detector. Table 4 provides the execution time of the compared methods, where the mediocre time performance of the proposed SSFAD is exposed. Such unideal time consuming probably is caused by the computational cost of matrix inversion operation and saliency weight calculation increasing with the size of the additional local window. Whatever, the ordinary time performance can hardly cover the superiorities of the proposed SSFAD towards hyperspectral anomaly detection.

4 Conclusions

In this paper, a novel dual-pipeline framework that extracted spatial and spectral features separately and then fused them adaptively was proposed for hyperspectral anomaly detection. In spectral domain, original spectral signal was first mapped to a local median-mean linear background, and then saliency weight and feature enhancement strategies were implemented to obtain an initial detection map. In spatial domain, a new detector was designed to fully excavate the similarity spatial information of local patches around center window. Finally, anomalies were detected by jointly considering the spectral and spatial detection maps. Experimental results on four real hyperspectral datasets confirmed that the proposed SSFAD method had superior background suppression ability and excellent detection performance than traditional anomaly detection methods.

References

- Zengfu Hou, Yu Chen, Kun Tan, and Peijun Du. Novel hyperspectral anomaly detection methods based on unsupervised nearest regularized subspace. *International Archives of the Photogrammetry, Remote Sensing & Spatial Information Sciences*, 42(3), 2018.
- Zengfu Hou and Wei Li. A joint morphological profiles and patch tensor change detection for hyperspectral imagery. *arXiv preprint arXiv:2201.08027*, 2022.

- Xiaobin Zhao, Zengfu Hou, Xin Wu, Wei Li, Pengge Ma, and Ran Tao. Hyperspectral target detection based on transform domain adaptive constrained energy minimization. *International Journal of Applied Earth Observation and Geoinformation*, 103:102461, 2021.
- Jingliang Hu, Lichao Mou, Andreas Schmitt, and Xiao Xiang Zhu. Fusionet: A two-stream convolutional neural network for urban scene classification using polsar and hyperspectral data. In *2017 Joint Urban Remote Sensing Event (JURSE)*, pages 1–4. IEEE, 2017.
- Alberto Villa, Jocelyn Chanussot, Jon Atli Benediktsson, and Christian Jutten. Spectral unmixing for the classification of hyperspectral images at a finer spatial resolution. *IEEE Journal of Selected Topics in Signal Processing*, 5(3): 521–533, 2010.
- Zengfu Hou, Wei Li, Lu Li, Ran Tao, and Qian Du. Hyperspectral change detection based on multiple morphological profiles. *IEEE Transactions on Geoscience and Remote Sensing*, 2021a.
- Zengfu Hou, Wei Li, Ran Tao, and Qian Du. Three-order tucker decomposition and reconstruction detector for unsupervised hyperspectral change detection. *IEEE Journal of Selected Topics in Applied Earth Observations and Remote Sensing*, 14:6194–6205, 2021b.
- Jun Liu, Zengfu Hou, Wei Li, Ran Tao, Danilo Orlando, and Hongbin Li. Multipixel anomaly detection with unknown patterns for hyperspectral imagery. *IEEE Transactions on Neural Networks and Learning Systems*, pages 1–11, 2021. doi:10.1109/TNNLS.2021.3071026.
- Zengfu Hou, Wei Li, Lianru Gao, Bing Zhang, Pengge Ma, and Junling Sun. A background refinement collaborative representation method with saliency weight for hyperspectral anomaly detection. In *IGARSS 2020-2020 IEEE International Geoscience and Remote Sensing Symposium*, pages 2412–2415. IEEE, 2020.
- Zengfu Hou, Li Wei, Ran Tao, and Weihua Shi. Collaborative representation with background purification and saliency weight for hyperspectral anomaly detection. *SCIENCE CHINA Information Sciences*, 65:112305, 2021c.
- Irving S Reed and Xiaoli Yu. Adaptive multiple-band cfar detection of an optical pattern with unknown spectral distribution. *IEEE Transactions on Acoustics, Speech, and Signal Processing*, 38(10):1760–1770, 1990.
- José Manuel Molero, Ester M Garzón, Inmaculada García, and Antonio Plaza. Analysis and optimizations of global and local versions of the rx algorithm for anomaly detection in hyperspectral data. *IEEE Journal of Selected Topics in Applied Earth Observations and Remote Sensing*, 6(2):801–814, 2013.
- Qiangdong Guo, Bing Zhang, Qiong Ran, Lianru Gao, Jun Li, and Antonio Plaza. Weighted-rxd and linear filter-based rxd: Improving background statistics estimation for anomaly detection in hyperspectral imagery. *IEEE Journal of Selected Topics in Applied Earth Observations and Remote Sensing*, 7(6):2351–2366, 2014.
- Heesung Kwon and Nasser M Nasrabadi. Kernel rx-algorithm: A nonlinear anomaly detector for hyperspectral imagery. *IEEE transactions on Geoscience and Remote Sensing*, 43(2):388–397, 2005.
- Wei Li and Qian Du. Collaborative representation for hyperspectral anomaly detection. *IEEE Transactions on Geoscience and Remote Sensing*, 53(3):1463–1474, 2014.
- Maryam Vafadar and Hassan Ghassemian. Hyperspectral anomaly detection using outlier removal from collaborative representation. In *2017 3rd International Conference on Pattern Recognition and Image Analysis (IPRIA)*, pages 13–19. IEEE, 2017.
- Hongjun Su, Zhaoyue Wu, Qian Du, and Peijun Du. Hyperspectral anomaly detection using collaborative representation with outlier removal. *IEEE Journal of Selected Topics in Applied Earth Observations and Remote Sensing*, 11(12): 5029–5038, 2018.
- Kun Tan, Zengfu Hou, Fuyu Wu, Qian Du, and Yu Chen. Anomaly detection for hyperspectral imagery based on the regularized subspace method and collaborative representation. *Remote sensing*, 11(11):1318, 2019a.
- Emmanuel J Candès, Xiaodong Li, Yi Ma, and John Wright. Robust principal component analysis? *Journal of the ACM (JACM)*, 58(3):1–37, 2011.
- Guangcan Liu, Zhouchen Lin, Shuicheng Yan, Ju Sun, Yong Yu, and Yi Ma. Robust recovery of subspace structures by low-rank representation. *IEEE transactions on pattern analysis and machine intelligence*, 35(1):171–184, 2012.
- Yang Xu, Zebin Wu, Zhihui Wei, Hongyi Liu, and Xiong Xu. A novel hyperspectral image anomaly detection method based on low rank representation. In *2015 IEEE International Geoscience and Remote Sensing Symposium (IGARSS)*, pages 4444–4447. IEEE, 2015a.
- Yubin Niu and Bin Wang. Hyperspectral anomaly detection based on low-rank representation and learned dictionary. *Remote Sensing*, 8(4):289, 2016.
- Kun Tan, Zengfu Hou, Donglei Ma, Yu Chen, and Qian Du. Anomaly detection in hyperspectral imagery based on low-rank representation incorporating a spatial constraint. *Remote Sensing*, 11(13):1578, 2019b.

- Yi Chen, Nasser M Nasrabadi, and Trac D Tran. Simultaneous joint sparsity model for target detection in hyperspectral imagery. *IEEE Geoscience and Remote Sensing Letters*, 8(4):676–680, 2011.
- Yang Xu, Zebin Wu, Jun Li, Antonio Plaza, and Zhihui Wei. Anomaly detection in hyperspectral images based on low-rank and sparse representation. *IEEE Transactions on Geoscience and Remote Sensing*, 54(4):1990–2000, 2015b.
- Tongkai Cheng and Bin Wang. Graph and total variation regularized low-rank representation for hyperspectral anomaly detection. *IEEE Transactions on Geoscience and Remote Sensing*, 58(1):391–406, 2019.
- Wei Li, Guodong Wu, and Qian Du. Transferred deep learning for anomaly detection in hyperspectral imagery. *IEEE Geoscience and Remote Sensing Letters*, 14(5):597–601, 2017. doi:10.1109/LGRS.2017.2657818.
- Weiyang Xie, Jie Lei, Baozhu Liu, Yunsong Li, and Xiuping Jia. Spectral constraint adversarial autoencoders approach to feature representation in hyperspectral anomaly detection. *Neural Networks*, 119:222–234, 2019.
- Chunhui Zhao and Lili Zhang. Spectral-spatial stacked autoencoders based on low-rank and sparse matrix decomposition for hyperspectral anomaly detection. *Infrared Physics & Technology*, 92:166–176, 2018.
- Xiaoqiang Lu, Wuxia Zhang, and Ju Huang. Exploiting embedding manifold of autoencoders for hyperspectral anomaly detection. *IEEE Transactions on Geoscience and Remote Sensing*, 58(3):1527–1537, 2019.
- Shaoyu Wang, Xinyu Wang, Liangpei Zhang, and Yanfei Zhong. Auto-ad: Autonomous hyperspectral anomaly detection network based on fully convolutional autoencoder. *IEEE Transactions on Geoscience and Remote Sensing*, 60:1–14, 2022. doi:10.1109/TGRS.2021.3057721.
- Chunhui Zhao, Xueyuan Li, and Haifeng Zhu. Hyperspectral anomaly detection based on stacked denoising autoencoders. *Journal of Applied Remote Sensing*, 11(4):042605, 2017.
- Maryam Imani. Rx anomaly detector with rectified background. *IEEE Geoscience and Remote Sensing Letters*, 14(8):1313–1317, 2017.
- Jie Lei, Weiyang Xie, Jian Yang, Yunsong Li, and Chein-I Chang. Spectral-spatial feature extraction for hyperspectral anomaly detection. *IEEE Transactions on Geoscience and Remote Sensing*, 57(10):8131–8143, 2019.
- Huihui Ju, Zhigang Liu, and Yang Wang. Hyperspectral anomaly detection incorporating spatial information. In *2018 Eighth International Conference on Image Processing Theory, Tools and Applications (IPTA)*, pages 1–5. IEEE, 2018.
- Xudong Kang, Xiangping Zhang, Shutao Li, Kenli Li, Jun Li, and Jon Atli Benediktsson. Hyperspectral anomaly detection with attribute and edge-preserving filters. *IEEE Transactions on Geoscience and Remote Sensing*, 55(10):5600–5611, 2017.
- Ahmad W Bitar, Loong-Fah Cheong, and Jean-Philippe Ovarlez. Sparse and low-rank matrix decomposition for automatic target detection in hyperspectral imagery. *IEEE Transactions on Geoscience and Remote Sensing*, 57(8):5239–5251, 2019.
- Ning Huiyan, Xiangrong Zhang, Huiyu Zhou, and Licheng Jiao. Hyperspectral anomaly detection via background and potential anomaly dictionaries construction. *IEEE Transactions on Geoscience and Remote Sensing*, 57(4):2263–2276, 2018.
- Yuxiang Zhang, Bo Du, Liangpei Zhang, and Shugen Wang. A low-rank and sparse matrix decomposition-based mahalanobis distance method for hyperspectral anomaly detection. *IEEE Transactions on Geoscience and Remote Sensing*, 54(3):1376–1389, 2015.
- James A Hanley and Barbara J McNeil. The meaning and use of the area under a receiver operating characteristic (roc) curve. *Radiology*, 143(1):29–36, 1982.